THE JOURNAL OF PHYSICAL CHEMISTRY B

ARTICLE

pubs.acs.org/JPCB

Valence Photoemission Spectra of Aqueous $Fe^{2+/3+}$ and $[Fe(CN)_6]^{4-/3-}$ and Their Interpretation by DFT Calculations

Robert Seidel,[†] Stephan Thürmer,[†] Jan Moens,[‡] Paul Geerlings,[‡] Jochen Blumberger,[*,§] and Bernd Winter[*,†]

[†]Helmholtz-Zentrum Berlin für Materialien und Energie, and BESSY, Albert-Einstein-Strasse 15, D-12489 Berlin, Germany

[‡]Faculty of Sciences, Department of General Chemistry, Free University of Brussels (VUB), Pleinlaan 2, 1050 Brussels, Belgium

[§]Department of Physics and Astronomy, University College London, London WC1E 6BT, United Kingdom

ABSTRACT: Aqueous solutions of ferrous and ferric iron ($Fe^{2+/3+}$) and of the iron−hexacyano complexes $[Fe(CN)_6]^{4-/3-}$ are studied by photoelectron spectroscopy using a liquid microjet in conjunction with synchrotron soft X-rays for ionization. For $Fe^{2+}(aq)$ we observe two well-resolved peaks at 7.09 and 9.16 eV electron binding energy (BE) that can be assigned to the iron−hexaaquo complex. For $Fe^{3+}(aq)$ we observe only one peak above the highest valence band of liquid water, at 10.08 eV BE. Interpreting the spectra in terms of the one-electron levels of Kohn−Sham density functional theory, we find that the two peaks for $Fe^{2+}(aq)$ originate from the energy splitting between the highest occupied β (= minority) spin level (Fe $d(t_{2g})$) and the five highest occupied α (= majority) spin levels (Fe $d(t_{2g})$ and $d(e_g)$). The peak for $Fe^{3+}(aq)$ arises from d-levels that are strongly mixed with the solvent. The spectra of the aqueous hexacyano complexes show a single strong peak at 6.11 and 7.52 eV BE for $[Fe(CN)_6]^{4-}$ and $[Fe(CN)_6]^{3-}$, respectively, originating from the highest occupied Fe $d(t_{2g})$ levels, and two further peaks at higher BE originating from the cyano ligands. The PE spectra of the reduced aquo and cyano ions are then used to obtain—solely on experimental grounds—values for the reorganization free energy of the oxidized ions. DFT/continuum calculations of this important parameter in the Marcus theory of oxidation reactions are in fairly good agreement with experiment.

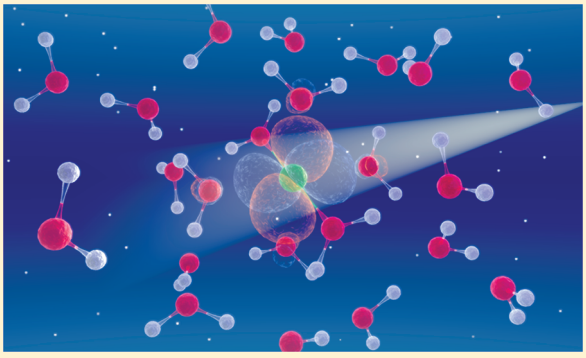

1. INTRODUCTION

The chemistry of transition metal (TM) ions in aqueous solution is manifold and complex,[1−13] but despite their enormous importance in many fields of chemistry, especially in catalysis, electro-, thermo-, photoredox-, and biochemistry, many aspects of the electronic structure interactions of TM ions with water are still not well understood. For instance, valence electron energies, which play a crucial role in chemical reactions of TM ions in aqueous solutions, are usually unknown. This lack is primarily due to previous experimental difficulties with detecting energies of electrons emitted from highly volatile samples. However, with the recent development of the vacuum liquid microjet for X-ray photoelectron (PE) spectroscopy, measurements can now be performed.[14] To date, valence PE studies have been reported from TM aqueous solutions for $Mn^{2+}(aq)$,[15] $Ru(bpy)_3^{2+}(aq)$,[16] and $Ni^{2+}(aq)$.[17] PE spectra from iron aqueous solutions have so far been measured for $K_3Fe(CN)_6(aq)$ and $K_4Fe(CN)_6(aq)$,[18] and via the BE of the latter complex, the charge-transfer-to-solvent (CTTS) energies and the BE of the solvated electron in water have been determined.[19]

We would like to mention that electronic structure and chemical bonding of first-row transition metal halide molecules have been explored intensively in the gas phase, also using PE spectroscopy. Specifically, the complex electronic energy level structure arising from electron correlation, spin−orbit, and spin−spin effects in those open-shell electron configurations has been exhaustively addressed.[20−22] In the present work, however, we are concerned with the situation where the halide ligand is replaced by the water ligand and the coordination complex interacts with the solvent.

Here we report a comparative soft X-ray photoelectron (PE) spectroscopy study of the valence electronic structure of ferrous (Fe^{2+}) and ferric iron (Fe^{3+}) in water and of the corresponding hexacyano complexes, $[Fe(CN)_6]^{4-}$ and $[Fe(CN)_6]^{3-}$, in aqueous solution. Both TM ion charge and ligand determine the solution's properties, such as solubility, color, complex stability, and magnetic behavior. While ferrous and ferric iron are high-spin complexes, the hexacyano compounds are low spin in their electronic ground state. Crystal field theory gives a simple yet intuitive qualitative explanation for the different magnetic behavior of hexaaquo and hexacyano complexes: the crystal field created by the aquo ligands is smaller than the spin pairing energy, and as a consequence, both the Fe $3d(t_{2g})$ and $3d(e_g)$ orbitals are filled, giving a high-spin configuration. By contrast, the cyanide ligand generates a strong crystal field due to its net charge and π-orbital interactions with the metal ion. Consequently, only the

Received: April 29, 2011
Revised: July 12, 2011
Published: August 02, 2011

Fe 3d(t_{2g}) levels are filled, and the ground state is a low-spin configuration.

The focus of the present work is on the experimental and computational determination of lowest electron binding energies, which are all of primarily TM ion character. Their binding energies (BEs) are expected to be well below those of any water-solvent electronic state. A specific question that we would like to investigate is whether the PE spectra can be used to obtain the splitting of 3d energy levels in aqueous $Fe^{2+/3+}$ complexes, a property that is usually obtained from electron (optical) absorption spectroscopy.[23] In our previous investigation of aqueous Mn^{2+} ($3d^5$ high-spin), we could indeed decompose the broad peak at the lowest electron BE into two peaks and interpreted them as arising from the Mn 3d(t_{2g}) and 3d(e_g) manifold of levels. However, for the case of Fe^{2+}(aq), we expect a more complicated situation since the 3d levels are now occupied by both α and β spin electrons. In addition to electron binding energy, we will also report experimental and computed reorganization free energies of aqueous Fe^{3+} and $[Fe(CN)_6]^{3-}$, a fundamental property in the Marcus theory of oxidation reactions.

Anticipating our results, we observe indeed two peaks in the PE spectrum of Fe^{2+}(aq) that originate from the metal 3d levels. However, according to Kohn−Sham density functional theory calculations, the levels are due to the energy splitting of α/β spin rather than d(t_{2g})/d(e_g) energy levels. The spectra of the cyano complexes exhibit rich features due to metal-d and ligand levels, which are well above the highest water valence band.

2. METHODS

2.1. Experimental Section. Photoemission measurements were performed from an 18 μm sized vacuum liquid jet[24] at the soft-X-ray U41 PGM undulator beamline of BESSY, Berlin. The jet velocity was approximately 100 ms^{-1}, and jet temperature was 6 °C. Electrons were detected normal to both the synchrotron light polarization vector and the flow of the liquid jet. A 100 μm diameter orifice that forms the entrance to the hemispherical electron energy analyzer is at an approximately 0.5 mm distance from the liquid jet—a short enough distance to ensure that detected electrons have not suffered from inelastic scattering with water gas-phase molecules around the small-sized liquid jet.[14,24,25] At operation conditions, the pressure in the interaction chamber was about 1.5×10^{-4} mbar. The energy resolution of the U41 beamline is better than 50 meV at the incident photon energies used here, and the resolution of the hemispherical energy analyzer is constant with kinetic energy (about 100 meV at 10 eV pass energy). The small focal size, $23 \times 12\ \mu m^2$, of the incident photon beam allows for matching spatial overlap with the liquid microjet, reducing the gas-phase contributions of the measured spectra to less than 5% for liquid water. The aqueous solutions were prepared using deionized water. $FeCl_2$ and $Fe(NO_3)_3$ nonahydrate salts were of 98% purity, and the $K_4Fe(CN)_6$ trihydrate and the $K_3Fe(CN)_6$ salts were of 99% purity. We used a (rather low) salt concentration of 0.25 molal (m) to suppress substitution of first-shell waters by counterions.

2.2. Theoretical Calculations. Computations were carried out for two models of aqueous Fe^{2+} and Fe^{3+}. In the first model, Fe and the six water molecules forming the first solvation shell were included in the QM calculation, and the remaining solvent was treated as a continuum. In the second model, the 12 water molecules of the second solvation shell were included in the QM calculation in addition to the first shell water molecules (i.e., a total of 18 water molecules). The initial structures for the 6 and 18 water molecule models were taken from a previous study[26] and reoptimized in vacuum using the all electron 6-311+g(d,p) basis set for metal and ligand atoms. Three common exchange-correlation functionals were used, PBE,[27] BLYP,[28,29] and B3LYP,[29,30] employing the local spin density approximation. Calculations were carried out for the experimental spin ground state (high spin, $S = 4/2$ and 5/2 for Fe^{2+} and Fe^{3+}, respectively). Frequency calculations were carried out to ensure that structures correspond to minima on the potential energy surface. Wave functions were checked to be free from internal instabilities.[31,32] The Kohn−Sham (KS) energy levels and the vertical and adiabatic ionization energies were calculated on the optimized structures using the cc-pVTZ basis set for the ligands and for Fe. They include the interaction energy with the solvent modeled as a continuum. For the equilibrium states Fe^{2+} and Fe^{3+}, the solute−solvent interaction was calculated using the polarizable continuum model (PCM),[33] which accounts for both the (fast) electronic and (slow) nuclear relaxation of the solvent. For the vertically oxidized and reduced states (denoted by a star * throughout the manuscript), the solute−solvent interaction energy was calculated using the nonequilibrium solvation method implemented in Gaussian03.[34] The latter accounts only for the electronic polarization of the solvent but not for the nuclear relaxation, thus describing vertical processes. Similar calculations were carried out for the cyano complexes, except that both geometry optimization and final energy calculations were carried out with the cc-pVTZ basis set. The Fe and the six CN^- ligands are treated quantum mechanically in the experimental spin ground state (low spin, $S = 0$ and 1/2 for $[Fe(CN)_6]^{4-}$ and $[Fe(CN)_6]^{3-}$, respectively) using the same density functionals and continuum models as for the aquo complexes. All calculations were carried out with the Gaussian03 software.[35] While wave function optimizations were straightforward for the species of the redox cycles of Fe^{2+}(aq) and the aqueous hexacyano complexes, all attempts to converge the orbitals of vertically ionized Fe^{3+}(aq) (i.e., Fe^{4+*}) were not successful. Thus, for Fe^{3+}(aq) we only report KS energy levels.

3. RESULTS AND DISCUSSION

3.1. PE Spectra. Valence photoelectron spectra from 0.25 m $FeCl_2$, $Fe(NO_3)_3$, $K_4Fe(CN)_6$, and $K_3Fe(CN)_6$ aqueous solutions, measured at a photon energy of 200 eV, are shown in Figure 1a−d (red curves). We also present PE spectra from suitable reference solutions, 0.5 m NaCl, 0.75 m $NaNO_3$, and neat water (blue curves), which are used to extract iron-related signal, by pairwise subtraction of spectra. Notice that the latter two concentrations were chosen to yield the same anion concentration as for the respective iron solutions. BEs displayed in Figure 1 are with respect to the vacuum level and were calibrated by the $1b_1$ BE of liquid water at 11.16 eV.[36] PE signals are normalized to the water $1b_2$ peak. Major peaks in the spectra are labeled by the solute or water orbitals from which electrons are emitted.[14,24] Here we are mainly interested in the solute contributions at BEs lower than the ionization onset of water, and we show that particular spectral region enlarged in the respective insets of Figure 1, again displaying the pairs of spectra. For the quantitative analysis of the low-energy solute PE spectra, we consider the differential spectra (iron solution minus reference spectrum) of Figure 2. Unconstrained Gaussian peak fitting of the spectra reveals peak positions and widths of the main spectral

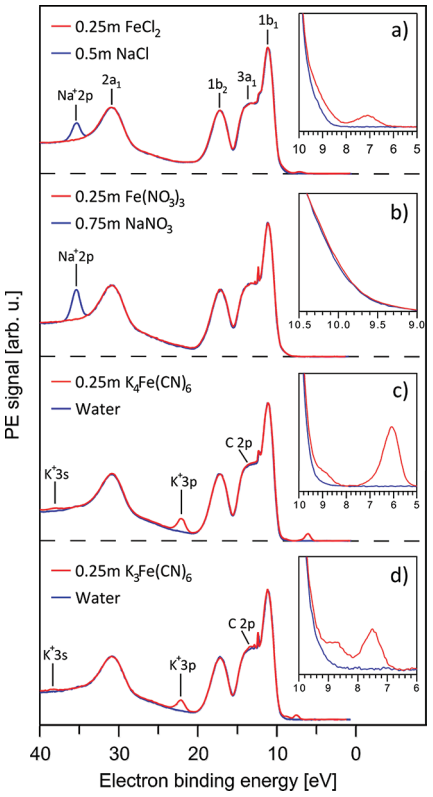

Figure 1. Valence photoelectron spectra of 0.25 m $FeCl_2$, $Fe(NO_3)_3$, $K_4Fe(CN)_6$, and $K_3Fe(CN)_6$ aqueous solutions (red curves) measured at 200 eV photon energy. Reference spectra from non-iron-containing solutions are shown in blue. Energies displayed are electron binding energies with respect to vacuum. Prominent water and solute PE features are labeled. Insets are zooms into the low-binding energy region.

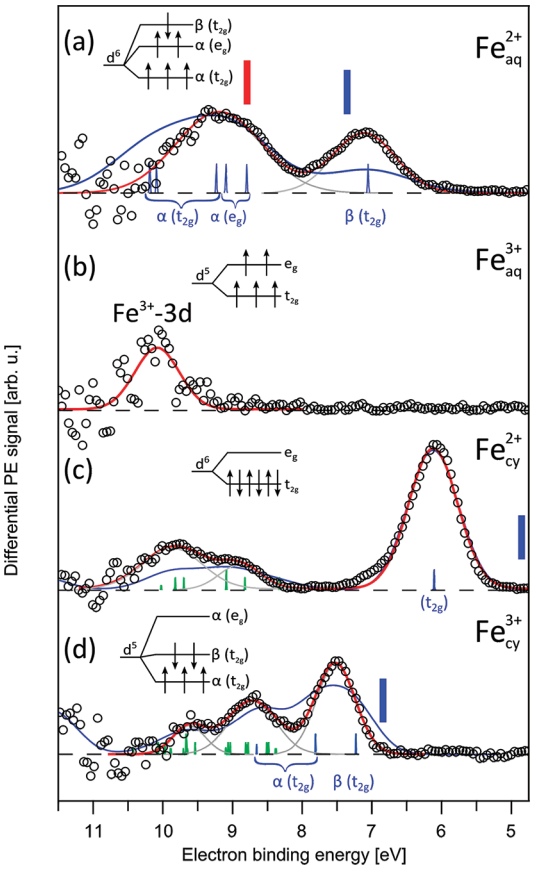

Figure 2. Enlarged view of the differential spectra (subtraction of the solution reference spectra from the iron-containing solution spectra) in the low-binding energy region from Figure 1. Open circles are experimental data; thin gray lines identify individual Gaussian peaks; and the red curves are the total fit to the respective experimental PE spectrum. Computed data are shown in blue and green (B3LYP, 18 water molecule system in panel (a), B3LYP in panels (c) and (d)). The spikes depicted in panels (a), (c), and (d) are the KS energy levels obtained after aligning the β (= minority) spin HOMO level in (a) and (d) and the HOMO level in (c) with the experimental peak at the lowest BE. Peak labels are explained in the text. Energy levels that have predominantly Fe-d character are shown in blue, and ligand levels are shown in green. The thin blue line is the total sum of the computed peaks broadened with a Gaussian of width 1.0 eV for (a), 0.82 eV for (c), and 0.6 eV for (d) full width at half-maximum. In (c) and (d) the metal states were weighted by a factor of 3 compared to the ligand states, justified by a larger ionization cross section for Fe-3d. Blue bars mark the calculated ionization energy, i.e., the difference in the total DFT energy of reduced and oxidized state at the equilibrium configuration of the reduced state. The red bar highlights the energy required for removing the α (e_g) electron from Fe^{2+}(aq). The electron occupation according to spin-unrestricted (a, b, and d) and spin-restricted (c) crystal field theory is shown schematically as insets in each panel.

contributions in the valence region of the solutions. The corresponding values are summarized in Table 1.

Fe^{2+}(aq). In the PE spectrum of Fe^{2+}(aq) (Figure 2a), we observe two peaks, at 7.09 and 9.16 eV BE, with a peak-area ratio of 1:1.88. We have carried out spin-unrestricted DFT calculations to interpret these peaks. In Figure 2a we show the Kohn−Sham energy levels obtained from the B3LYP calculations with 18 explicit water molecules (thin spikes in blue). Calculated levels have been shifted by 1.44 eV to higher BEs such that the highest energy level of the β (= minority) spin electron aligns with the experimental peak at 7.09 eV. This latter level is composed of a Fe 3d(t_{2g}) orbital and is entirely localized on the hexaaquo complex, not extending to the second solvation shell. We find that the position of the five highest α (= majority) spin orbitals coincides remarkably well with the broad experimental peak at 9.16 eV. All five levels are again localized on the hexaaquo complex, with the two highest levels composed of Fe 3d(e_g) orbitals and the three lower levels composed of Fe 3d(t_{2g}) orbitals (see labels in Figure 2a). Modeling the PE spectrum by Gaussians of 1.0 eV full width at half maximum, centered at the computed peak positions, we obtain the blue curve of Figure 2a. Although the peak-area ratio differs from experiment, the difference of the two maxima, 2.08 eV, is in very good agreement with the experimentally obtained 2.07 eV.

The DFT energy levels in Figure 2a can be interpreted in terms of a spin-unrestricted crystal field model as shown in the inset. In this model the α electrons are assumed to be separated from the β electron by a spin-pairing energy P, and each spin manifold is split into degenerate t_{2g} and e_g levels. We note, however, that according to the DFT calculations the α-spin Fe 3d(t_{2g}) levels are not degenerate; in fact, the highest α Fe 3d(t_{2g}) level is closer to the Fe 3d(e_g) levels than to the other two Fe 3d(t_{2g}) levels. This is certainly related to the departure from the ideal octahedral symmetry in the structure-optimized complex. The Fe^{2+}(aq) complex is distorted along one of the molecular axes resulting in a compressed octahedron with 2.15 Å for the equatorial bonds and

Table 1. Lowest Experimental Binding Energy (E_b), Computed Ionization Energy (ΔE_R), and Reorganization Free Energies (λ_O) of Aqueous $Fe^{2+/3+}$ and $Fe(CN)_6^{4-/3-}$[a]

	ionization energy in [eV]			reorganization energy (λ_O) in [eV]		
complex	exp (E_b)	calc (ΔE_R)		exp	calc	
Fe^{2+}	7.09 (1.08 ± 0.08)	$[Fe(H_2O)_6]^{2+}$	7.37[b]	2.04	$[Fe(H_2O)_6]^{3+}$	1.71[b]
			7.42[c]			1.70[c]
			8.12[d]			1.95[d]
		$[Fe(H_2O)_{18}]^{2+}$	6.59[b]		$[Fe(H_2O)_{18}]^{3+}$	1.72[b]
			6.67[c]			1.66[c]
			7.38[d]			1.89[d]
Fe^{3+}	10.08	--	--	--	--	--
$[Fe(CN)_6]^{4-}$	6.11 (0.82 ± 0.02)	$[Fe(CN)_6]^{4-}$	5.02[b]	1.47	$[Fe(CN)_6]^{3-}$	1.12[b]
			4.79[c]			1.14[c]
			4.82[d]			1.24[d]
$[Fe(CN)_6]^{3-}$	7.52 (0.67 ± 0.03)	$[Fe(CN)_6]^{3-}$	6.51[b]	--	--	--
			6.83[d]			--

[a] Values given in parentheses are experimental peak widths (full width at half maximum). [b] PBE. [c] BLYP. [d] B3LYP.

2.13 Å for the axial bond lengths as obtained at the B3LYP level of theory. Disregarding this complication, we estimate an effective crystal field splitting energy for the α electrons as the difference between the center of the two Fe 3d(e_g) levels and the center of the two lowest Fe 3d(t_{2g}) levels. The value we obtain, 1.19 eV, is close to the tabulated experimental values obtained from optical spectroscopy, 1.24[23]−1.29 eV.[37] The spin-pairing energy obtained from the difference between the β-spin Fe 3d(t_{2g}) KS level and the center of the two lowest Fe 3d(t_{2g}) levels, P = 3.1 eV, is significantly larger than the ligand-field splitting energy as expected for an ion with a high-spin ground state.

In summary, our DFT calculations suggest that the two peaks at lowest BE in the photoemission spectrum of aqueous Fe^{2+}(aq) are due to the energy gap between the β-spin highest occupied molecular orbital, HOMO (Fe 3d(t_{2g})), and the manifold of the five highest α-spin levels (Fe 3d(e_g) + Fe 3d(t_{2g})). Indeed, well-resolved ionization energies for removal of α- and β- spin electrons have been reported before for gaseous transition metal complexes, e.g., in ref 20. However, this is the first time that this important feature is observed in the photoemission spectrum of an aqueous transition metal ion.

Fe^{3+}(aq). Turning to the differential PE spectrum for Fe^{3+}(aq) at the photon energy of 200 eV (Figure 2b), we find a single peak at 10.08 eV BE, which lies right at the onset of the water $1b_1$ band. This peak is clearly a signature of the Fe 3d levels because it is observed in the solute minus solvent spectrum. DFT calculations at the B3LYP level show that all five α-spin 3d-levels (including the HOMO) strongly mix with water levels of the first *and* second solvation shell, which is consistent with the small gap between the experimental Fe 3d peak and the highest valence band of liquid water.

$[Fe(CN)_6]^{4-}$(aq) and $[Fe(CN)_6]^{3-}$(aq). For the low-spin hexacyano complexes we observe single strong peaks at 6.11 and 7.52 eV BE, respectively, which according to crystal field theory and DFT calculations can be assigned to the Fe 3d(t_{2g}) levels (Figure 2c and d). For the spin-paired $[Fe(CN)_6]^{4-}$(aq) complex, all three doubly occupied d(t_{2g}) levels are degenerate as depicted by a single blue spike at the lowest binding energy in Figure 2c. Unrestricted DFT calculations for $[Fe(CN)_6]^{3-}$(aq) indicate that the Fe 3d(t_{2g}) levels split into a pair of degenerate β levels and a pair of degenerate α levels, separated by a spin-pairing energy of 0.6 eV, as indicated by the two spikes at the lowest BE in Figure 2d. Here we have shifted the absolute KS energy levels to higher energies, by 1.39 eV for Fe^{2+}(cyan) and by 0.65 eV for Fe^{3+}(cyan), to match the experimental peak positions. The third α level strongly mixes with ligand orbitals, leading to lower binding energies.

In addition to Fe 3d peaks, two further peaks, at energies below the water bands, can be identified in the experimental spectra, at 8.88 and 9.82 eV for $[Fe(CN)_6]^{4-}$ (Figure 2c) and at 8.71 and 9.63 eV for $[Fe(CN)_6]^{3-}$ (Figure 2d), respectively. These pairs of peaks are at similar positions for the two iron−cyano complexes and are tentatively attributed to the π-orbitals of the cyano ligands. This assignment is supported by our comparative PE measurements of the CN^- molecule in water, exhibiting a single but broad PE peak (fwhm ∼1 eV) at 9.44 eV BE (not shown). We argue that the observed peak split and energy shifts in the case of the metal-coordination complexes result from the interaction of the cyanide ligands with the central metal ion (e.g., π-back bonding), and the seemingly narrower peak widths as compared to CN^-(aq) likely reflect the steric constraint (rigid ligands). Specifically, our calculations for $Fe(CN)_6^{4-}$(aq) yield two sets of spin-paired ligand π-orbitals centered at 2.8 and 3.6 eV below the HOMO energy level (green spikes in Figure 2c). Both energies match the positions of the second and third peak in the experimental spectrum at 2.8 and 3.7 eV below the HOMO peak very well, corroborating the above experimental assignment. For $Fe(CN)_6^{3-}$(aq), we also find two sets of ligand π-orbitals centered at 1.3 and 2.3 eV below the HOMO energy level (green spikes in Figure 2d) matching well the experimental peak positions at 1.2 and 2.1 eV below the HOMO peak. As mentioned above, the calculations predict that the third Fe 3d(t_{2g}) α level overlaps with the manifold of ligand levels at 2.1 eV below the HOMO level, which explains why this peak has a higher intensity for $Fe(CN)_6^{3-}$(aq) than for $Fe(CN)_6^{4-}$(aq).

3.2. Lowest Vertical Ionization Energies. In the calculations discussed above, we have used Kohn−Sham energy levels to interpret the PE spectra. It is well-known, however, that the absolute value of the highest KS level is not equal to the lowest

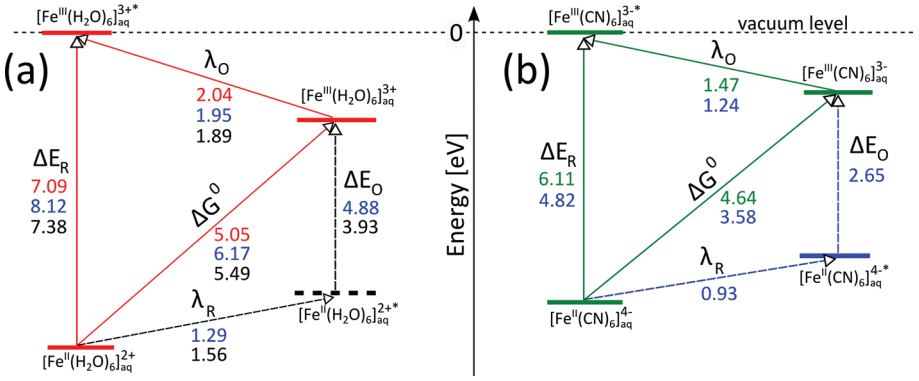

Figure 3. Energy-level diagram for (a) aqueous $Fe^{2+/3+}$—aquo and (b) aqueous $Fe^{2+/3+}$—hexacyano redox pairs. The vacuum level at 0 eV is shown by a dashed line. Experimental values are shown in red (a) and in green (b), respectively. Blue and black numbers correspond to results from B3LYP/continuum calculations including only the first solvation shell explicitly and including first plus second explicit shells, respectively. Indicated values either are taken from Table 1 or have been addressed in the text.

ionization potential due to the approximate nature of the exchange-correlation functional. Moreover, for very accurate treatment of the experimental data, spin−orbit coupling should in principle be included in the calculations. Here we have circumvented the former problem simply by aligning the computed levels with the experimental peak position at the lowest BE and considering only relative orbital energies.

Absolute vertical ionization energies can be obtained by calculating the state energy difference between the oxidized (E_O) and reduced state (E_R) at fixed nuclear configuration of the reduced state, giving $\Delta E_R = E_O\ (S = 5/2) - E_R\ (S = 4/2)$. The results are summarized in Table 1, and the best values obtained are depicted by blue bars in Figure 2. We find that vertical ionization energies depend rather strongly on the number of explicit water molecules included in the QM region. In the case of $Fe^{2+}(aq)$, when going from 6 to 18 water molecules, ΔE_R decreases by about 0.7−0.8 eV irrespective of the functional used. This shows that the interactions between strongly polarized first-shell water molecules and the second solvation shell cannot be accurately modeled with a continuum representation. A similar observation was made in ref 38. Using an extended solvation model comprising the first and the second solvation shells (18 water), the ionization potential of $Fe^{2+}(aq)$ at the B3LYP level, 7.38 eV, is in reasonably good agreement with the experimental peak position at 7.09 eV BE. GGA functionals underestimate ionization energy considerably, which is also the reason why we have used the B3LYP functional in combination with the 18-water-molecule system to interpret the PE spectra of $Fe^{2+}(aq)$ and $Fe^{3+}(aq)$ above. We have also calculated the second-lowest binding energy, corresponding to ionization of the α electron by evaluating the state energy difference between $E_O\ (S = 3/2)$ and $E_R\ (S = 4/2)$. For the 18-water-model of $Fe^{2+}(aq)$ we obtain 8.79 eV at the B3LYP level of theory (indicated by a red bar in Figure 2a), which is in reasonable agreement with the position of the second-highest peak in the experimental spectrum (9.16 eV). Thus, the state energy differences as well as the KS energies support our assignment of the $Fe^{2+}(aq)$ spectrum.

Turning to the aqueous iron−cyano complexes, we find that DFT calculations at the B3LYP and PBE level underestimate the electron binding energy considerably, by about 1 eV with respect to the lowest experimental BE. The calculated energies are marked by blue bars in Figures 2c and 2d, respectively. The deviations are slightly larger for the more negatively charged ion $Fe(CN)_6^{4-}$ than for $Fe(CN)_6^{3-}$. While part of this error is likely to be due to deficiencies in the functional, some of the error could be related to the modeling of the aqueous solution. In experiment, positively charged counterions possibly form contact pairs with the cyano complex, thereby modifying the local electric field at the iron site. This could lead to an increase in ionization energy relative to the pure aqueous solution modeled in the computations. Related effects of charge compensation/neutralization have been recently explored for different charge states of glycine in water.[39]

3.3. Reorganization Free Energies. The lowest electron binding energies in the PE spectra can be used to extract experimental reorganization free energies, one of the three parameters that determine the rate of oxidation reactions according to Marcus theory.[40] In essence, the reorganization free energy λ_O measures the free energy change required to rearrange the solute and the solvent from the equilibrium configuration of the initial charge state (e.g., reduced state) to the equilibrium configuration of the final charge state (e.g., oxidized state) while remaining on the same potential energy surface. It is thus the difference between the vertical (ΔE_R) and adiabatic ionization or oxidation free energy (ΔG^0)[15,16,41,42]

$$\lambda_O = \Delta E_R - \Delta G^0 \quad (1)$$

where the subscript "O" indicates that the reorganization free energy is for the oxidized state.[15,16] Experimentally, the vertical ionization energy can be identified with the peak position of the HOMO in the PE spectrum, E_b, corrected for the potential difference between the solution and vapor phase, $e\Delta\kappa$, $\Delta E_R = E_b + e\Delta\kappa$. The surface potential term is expected to be small (<10 meV for pure water jets[14]) and is thus neglected, i.e., $\Delta E_R \approx E_b$. The relation between ΔE_R and ΔG^0 is depicted in the energy-level diagram of Figure 3 for ionization of ground state $Fe^{2+}(aq)$ (a) and $[Fe(CN)_6]^{4-}(aq)$ (b). Vertical ionization from the HOMO level of these ions requires an energy ΔE_R and produces the oxidized states $Fe^{3+}(aq)^*$ and $[Fe(CN)_6]^{3-}(aq)^*$. The star (*) indicates that the nuclei have not relaxed in response to the change in oxidation state. The free energy released by the subsequent reorganization of the nuclei to the equilibrium configuration of the oxidized state is λ_O. The sum of the two processes, vertical ionization of the reduced state and reorganization free energy of the oxidized state, gives the adiabatic free

dx.doi.org/10.1021/jp203997p | J. Phys. Chem. B 2011, 115, 11671–11677

energy difference ΔG^0. Values of λ_O determined along this route are presented in Table 1. Here we have used ΔG^0 = 5.05 and 4.64 eV for the absolute oxidation free energy of $Fe^{2+/3+}(aq)$ and $[Fe(CN)_6]^{4-/3-}(aq)$, respectively. These values were obtained from the corresponding standard reduction potentials, 0.77 and 0.36 eV, respectively, using a value of 4.28 eV[43] for the absolute potential of the standard hydrogen electrode. Inserting the HOMO BEs from the measured PE spectra and the ΔG^0 values into eq 1, we obtain λ_O = 2.04 and 1.47 eV for $Fe^{3+}(aq)$ and $[FeCN)_6]^{3-}(aq)$, respectively (assuming $e\Delta\kappa$ = 0). The different reorganization energies of $Fe^{3+}(aq)$ and $Fe(CN)_6^{3-}(aq)$ can be explained by the small changes in the Fe−CN bond lengths upon reduction as compared to the more flexible water ligands of $Fe^{3+}(aq)$ which rearrange considerably upon reduction.

In principle, λ_O can be extracted solely from the PE spectra, i.e., without the use of electrochemical reduction potentials. This is because in Marcus theory the reorganization free energy can be related to the width σ of the thermal fluctuations of the energy gap[44]

$$\lambda_O = \sigma^2/(2k_BT) \quad (2)$$

where k_B is the Boltzmann constant, and T is the temperature. Here the energy gap is the energy for ionization from the highest occupied electronic state, and σ^2 is the variance of the corresponding Gaussian distributed spectral intensity. Gaussian fitting reveals experimental peak widths σ = 0.46 eV for $Fe^{2+}(aq)$ and 0.35 eV for Fe^{2+}(cyano), resulting in reorganization energies of 4.1 and 2.3 eV, respectively. These values are significantly larger than the values obtained via the "electrochemical route" (eq 1) and should be regarded with much caution. In the case of Fe^{2+}(cyano), the large width could be caused by electronic broadening by the three occupied t_{2g} levels. However, this argument may not hold for $Fe^{2+}(aq)$, where the peak at the lowest binding energy is interpreted as arising from a single electronic level. Some of the discrepancy could also be due to uncertainties in the fitting procedure and deviations from non-Gaussian peak shapes. As the reorganization free energy goes with the square of the width, it is rather sensitive to small variations in σ.

The DFT calculations reproduce the experimental λ_O obtained according to eq 1 well, 1.89 (18-water-model for $Fe^{2+/3+}(aq)$) and 1.24 eV, respectively, at the B3LYP level. We find that the computed values show much weaker dependence on system size and type of functional than ionization energies. λ_O changes by less than 0.06 eV when going from the 6- to the 18-water-molecule model for $Fe^{2+}(aq)$. The difference between GGA and B3LYP values is still significant but not more than 0.25 eV. Again, the B3LYP value is closest to the experimental value obtained from the PE spectroscopy data, underestimating the latter by only 0.15 ($Fe^{3+}(aq)$, 18 waters) and 0.23 eV ($[Fe(CN)_6]^{3-}$). Similar or even smaller errors were reported in our previous investigations for aqueous $Ru(bpy)_3^{3+}$[16] and Mn^{3+},[15] showing that computation and experiment give rather consistent results for this important redox property.

4. CONCLUSIONS

We have reported energy-resolved valence PE spectra of $Fe^{2+/3+}$ and $[Fe(CN)_6]^{4-/3-}$ in aqueous solution. Subtracting the photoemission intensity of solutions with and without the metal complexes, we found that all four ions exhibit solute levels above the highest valence band of liquid water. While for the low-spin hexacyano complexes the interpretation of the solute levels was straightforward, this was less the case for the high-spin hexaquo complexes. For $Fe^{3+}(aq)$ we found only a single peak at the valence band edge of liquid water due to Fe 3d levels. According to Kohn−Sham DFT calculations, these levels strongly mix with the solvent, which makes an interpretation in terms of crystal field theory difficult. For $Fe^{2+}(aq)$ the two peaks at the lowest binding energy were interpreted to originate from the energy level splitting of α and β spin levels rather than from e_g/t_{2g} level splitting. This interpretation is supported by the results of Kohn−Sham density functional calculations and the fact that the large separation of the two peaks is not consistent with common values for the crystal field splitting of this ion. This finding implies that the simple (spin restricted) crystal field picture of Fe^{2+} that is often found in textbooks is even qualitatively not correct. A spin unrestricted crystal field model as shown in Figure 3 is more appropriate to describe the electronic structure of this ion.

AUTHOR INFORMATION

Corresponding Author

*E-mail: j.blumberger@ucl.ac.uk; bernd.winter@helmholtz-berlin.de.

ACKNOWLEDGMENT

R.S., S.T., and B.W. thank the staff of BESSY for assistance, and B.W. acknowledges support from the DFG (project WI 1327/3-1). J.M. thanks the Fund for Scientific Research Flanders (FWO) for a predoctoral (Aspirant) fellowship. J.B. acknowledges The Royal Society for a University Research Fellowship and the computer support at the Department of Chemistry, University of Cambridge.

REFERENCES

(1) Greenwood, N. N.; Earnshaw, A. *Chemistry of the elements*, 2nd ed.; Butterworth-Heinemann: Oxford, 1997.
(2) Ohtaki, H.; Radnai, T. *Chem. Rev.* **1993**, *93*, 1157.
(3) Helm, L.; Merbach, A. E. *Chem. Rev.* **2005**, *105*, 1923.
(4) Rotzinger, F. P. *Chem. Rev.* **2005**, *105*, 2003.
(5) Moens, J.; Roos, G.; Jaque, P.; Proft, F.; Geerlings, P. *Chem. Eur. J.* **2007**, *13*, 9331.
(6) Cramer, C. J.; Truhlar, D. G. *Phys. Chem. Chem. Phys.* **2009**, *11*, 10757.
(7) Oberhofer, H.; Blumberger, J. *Angew. Chem., Int. Ed.* **2010**, *49*, 3631.
(8) Blumberger, J. *J. Am. Chem. Soc.* **2008**, *130*, 16065.
(9) Tateyama, Y.; Blumberger, J.; Ohno, T.; Sprik, M. *J. Chem. Phys.* **2007**, *126*, 204506.
(10) Blumberger, J.; Tavernelli, I.; Klein, M. L.; Sprik, M. *J. Chem. Phys.* **2006**, *124*, 64507.
(11) Blumberger, J.; Tateyama, Y.; Sprik, M. *Comput. Phys. Commun.* **2005**, *169*, 256.
(12) Hofer, T. S.; Rode, B. M.; Pribil, A. B.; Randolf, B. R. *Adv. Inorg. Chem.* **2010**, *62*, 143.
(13) Leung, K.; Nielsen, I. M. B.; Sai, N.; Medforth, C.; Shelnutt, J. A. *J. Phys. Chem. A* **2010**, *114*, 10174.
(14) Winter, B.; Faubel, M. *Chem. Rev.* **2006**, *106*, 1176.
(15) Moens, J.; Seidel, R.; Geerlings, P.; Faubel, M.; Winter, B.; Blumberger, J. *J. Phys. Chem. B* **2010**, *114*, 9173.
(16) Seidel, R.; Faubel, M.; Winter, B.; Blumberger, J. *J. Am. Chem. Soc.* **2009**, *131*, 16127.
(17) Seidel, R.; Thürmer, S.; Winter, B. *Phys. Chem. Lett.* **2011**, *2*, 633.

(18) Weber, R. *Photoelectron spectroscopy of liquid water and aqueous solutions in free microjets using synchrotron radiation*, 1999-10 ed.; Freie Universität: Berlin, 2003; Vol. Dissertation.
(19) Siefermann, K. R.; Liu, Y. X.; Lugovoy, E.; Link, O.; Faubel, M.; Buck, U.; Winter, B.; Abel, B. *Nature Chem.* **2010**, *2*, 274.
(20) Wang, L. S.; Niu, B.; Lee, Y. T.; Shirley, D. A. *J. Chem. Phys.* **1990**, *93*, 957.
(21) Berkowitz, J.; Streets, D. G.; Garritz, A. *J. Chem. Phys.* **1979**, *70*, 1305.
(22) Macnaughton, R. M.; Bloor, J. E.; Sherrod, R. E.; Schweitzer, G. K. *J. Electron Spectrosc. Relat. Phenom.* **1981**, *22*, 1.
(23) Figgis, B. N.; Hitchman, M. A. *Ligand Field Theory and Its Applications*; Wiley-VCH: New York, 2000.
(24) Winter, B. *Nucl. Instrum. Methods A* **2009**, *601*, 139.
(25) Faubel, M.; Steiner, B.; Toennies, J. P. *J. Chem. Phys.* **1997**, *106*, 9013.
(26) Uudsemaa, M.; Tamm, T. *J. Phys. Chem. A* **2003**, *107*, 9997.
(27) Perdew, J. P.; Burke, K.; Ernzerhof, M. *Phys. Rev. Lett.* **1996**, *77*, 3865.
(28) Becke, A. D. *Phys. Rev. A* **1988**, *38*, 3098.
(29) Lee, C. T.; Yang, W. T.; Parr, R. G. *Phys. Rev. B* **1988**, *37*, 785.
(30) Becke, A. *J. Chem. Phys.* **1993**, *98*, 5648.
(31) Seeger, R.; Pople, J. A. *J. Chem. Phys.* **1977**, *66*, 3045.
(32) Bauernschmitt, R.; Ahlrichs, R. *J. Chem. Phys.* **1996**, *104*, 9047.
(33) Tomasi, J.; Mennucci, B.; Cammi, R. *Chem. Rev.* **2005**, *105*, 2999.
(34) Cossi, M.; Barone, V. *J. Chem. Phys.* **2000**, *112*, 2427.
(35) Frisch, M. J.; Trucks, G. W.; Schlegel, H. B.; Scuseria, G. E.; Robb, M. A.; Cheeseman, J. R.; Scalmani, G.; Barone, V.; Mennucci, B.; Petersson, G. A.; Nakatsuji, H.; Caricato, M.; Li, X.; Hratchian, H. P.; Izmaylov, A. F.; Bloino, J.; Zheng, G.; Sonnenberg, J. L.; Hada, M.; Ehara, M.; Toyota, K.; Fukuda, R.; Hasegawa, J.; Ishida, M.; Nakajima, T.; Honda, Y.; Kitao, O.; Nakai, H.; Vreven, T.; Montgomery, J.; Peralta, J. E.; Ogliaro, F.; Bearpark, M.; Heyd, J. J.; Brothers, E.; Kudin, K. N.; Staroverov, V. N.; Kobayashi, R.; Normand, J.; Raghavachari, K.; Rendell, A.; Burant, J. C.; Iyengar, S. S.; Tomasi, J.; Cossi, M.; Rega, N.; Millam, J. M.; Klene, M.; Knox, J. E.; Cross, J. B.; Bakken, V.; Adamo, C.; Jaramillo, J.; Gomperts, R.; Stratmann, R. E.; Yazyev, O.; Austin, A. J.; Cammi, R.; Pomelli, C.; Ochterski, J. W.; Martin, R. L.; Morokuma, K.; Zakrzewski, V. G.; Voth, G. A.; Salvador, P.; Dannenberg, J. J.; Dapprich, S.; Daniels, A. D.; Farkas, Ö.; Foresman, J. B.; Ortiz, J. V.; Cioslowski, J.; Fox, D. J. *Gaussian 09*, revision A.1 ed.; Gaussian Inc.: Wallingford CT, 2009.
(36) Winter, B.; Weber, R.; Widdra, W.; Dittmar, M.; Faubel, M.; Hertel, I. V. *J. Phys. Chem. A* **2004**, *108*, 2625.
(37) Riedel, E.; Janiak, C. *Anorganische Chemie*; Walter de Gruyter: Berlin, 2004.
(38) Jaque, P.; Marenich, A. V.; Cramer, C. J.; Truhlar, D. G. *J. Phys. Chem. C* **2007**, *111*, 5783.
(39) Ottosson, N.; Borve, K. J.; Spangberg, D.; Bergersen, H.; Saethre, L. J.; Faubel, M.; Pokapanich, W.; Öhrwall, G.; Björneholm, O.; Winter, B. *J. Am. Chem. Soc.* **2011**, *133*, 3120.
(40) Marcus, R. A. *J. Chem. Phys.* **1965**, *43*, 679.
(41) Delahay, P.; Dziedzic, A. *J. Chem. Phys.* **1984**, *80*, 5793.
(42) Watanabe, I.; Ono, K.; Ikeda, S. *Bull. Chem. Soc. Jpn.* **1991**, *64*, 352.
(43) Isse, A. A.; Gennaro, A. *J. Phys. Chem. B* **2010**, *114*, 7894.
(44) Tateyama, Y.; Blumberger, J.; Sprik, M.; Tavernelli, I. *J. Chem. Phys.* **2005**, *122*, 234505.